Communication: XUV transient absorption spectroscopy of iodomethane and iodobenzene photodissociation

L. Drescher, M. C. E. Galbraith, G. Reitsma, J. Dura, N. Zhavoronkov, S. Patchkovskii, M. J. J. Vrakking, and J. Mikosch

Citation: The Journal of Chemical Physics **145**, 011101 (2016); doi: 10.1063/1.4955212
View online: http://dx.doi.org/10.1063/1.4955212
View Table of Contents: http://aip.scitation.org/toc/jcp/145/1
Published by the American Institute of Physics

Communication: XUV transient absorption spectroscopy of iodomethane and iodobenzene photodissociation

L. Drescher, M. C. E. Galbraith, G. Reitsma, J. Dura, N. Zhavoronkov, S. Patchkovskii, M. J. J. Vrakking, and J. Mikosch[a)]
Max-Born-Institut für nichtlineare Optik und Kurzzeitspektroskopie, Max-Born-Strasse 2A, 12489 Berlin, Germany

(Received 6 May 2016; accepted 22 June 2016; published online 6 July 2016)

Time-resolved extreme ultraviolet (XUV) transient absorption spectroscopy of iodomethane and iodobenzene photodissociation at the iodine pre-$N_{4,5}$ edge is presented, using femtosecond UV pump pulses and XUV probe pulses from high harmonic generation. For both molecules the molecular core-to-valence absorption lines fade immediately, within the pump-probe time-resolution. Absorption lines converging to the atomic iodine product emerge promptly in CH_3I but are time-delayed in C_6H_5I. We attribute this delay to the initial $\pi \rightarrow \sigma^*$ excitation in iodobenzene, which is distant from the iodine reporter atom. We measure a continuous shift in energy of the emerging atomic absorption lines in CH_3I, attributed to relaxation of the excited valence shell. An independent particle model is used to rationalize the observed experimental findings. *Published by AIP Publishing.* [http://dx.doi.org/10.1063/1.4955212]

Studies of chemical dynamics can benefit from the vibrant field of attosecond science[1] in many intriguing ways. The short duration of attosecond pulses implies broad and continuous frequency spectra with photon energies extending into the extreme ultraviolet (XUV), well suited for inner-shell absorption measurements in molecules.[2] Core-to-valence transitions are element-specific probes of the intramolecular local chemical environment, since an electron from a highly localized and energetically distinct core orbital is lifted to a hole in the valence shell, affected by chemical bonding. Core-to-valence transitions appear just below the ionization edges in the molecular absorption spectrum and are targeted by NEXAFS (Near Edge X-Ray Absorption Fine Structure) spectroscopy.[3] With the development of ultrashort XUV and X-ray pulses from high harmonic generation (HHG), slicing of synchrotron radiation, and free-electron lasers, this powerful tool of chemical structure analysis is currently being translated to the ultrafast time domain.[4–9] Table-top transient absorption studies with attosecond pulses and attosecond pulse trains (APTs) from HHG benefit from their appealing temporal and spectral properties.[10–14]

Here we probe the pre-$N_{4,5}$ edge region of iodine around 50 eV photon energy by transient XUV absorption of an APT. These transitions originate in the outermost 4d core shell in the iodine atom. We study photodissociation of iodomethane (CH_3I) and iodobenzene (C_6H_5I) in the A-band, pumped by a UV femtosecond laser pulse centered around 265 nm wavelength. Comparing transient XUV absorption of the well-explored photodissociation of these two molecules[15,16] promises to be particularly interesting, due to the intramolecular location of the valence shell hole created by the UV pump pulse. In CH_3I the dominant transition originates from promotion of an electron from a non-bonding (n) iodine orbital to an anti-bonding (σ^*) orbital localized on the C–I bond. In C_6H_5I, the dominant $\pi \rightarrow \sigma^*$ excitation involves the phenyl π orbital, which is distant from the iodine reporter atom.

Photodissociation of CH_3I was recently examined using a very similar experimental scheme. Through subtraction of the dominant transitions, Attar *et al.*[17] have found transient core-to-valence excitations at distinct energies. In contrast, we interpret our CH_3I results as the immediate emergence of a persisting new target state for XUV absorption upon molecular $n \rightarrow \sigma^*$ UV excitation. During dissociation, the molecular orbitals separate into atomic orbitals of iodine and molecular orbitals of the methyl fragment. This causes the UV-created hole in the valence shell to adjust, leading to a time-dependent shift in the XUV transition energy.

A-band excitation in CH_3I is split by the strong spin-orbit interaction into three overlapping states $^3Q_1$ (E), $^3Q_{0^+}$ (A_1), and $^1Q_1$ (E), dipole-allowed from the A_1 ground state.[18] While the $\tilde{X}\,A_1 \rightarrow {}^3Q_{0^+}$ transition carries the majority of the oscillator strength at 265 nm,[15,19] a non-adiabatic crossing with the higher-lying $^1Q_1$ state is encountered upon elongation of the C–I bond (see Fig. 1(a)), leading to population redistribution.[20] Asymptotically, the $^1Q_1$ state connects to ground-state I ($^2P_{3/2}$), while the $^3Q_{0^+}$ state leads to spin-orbit excited I* ($^2P_{1/2}$).

An apparatus usually used for photoion and -electron spectroscopy with short APTs and intense IR fields[21] was adapted for the present work. XUV pulses were generated via HHG in argon by a 6 fs duration laser pulse, obtained by spectral broadening in a neon-filled hollow-core fiber and chirped-mirror compression. UV pulses were produced by third harmonic generation of the 35 fs duration pulses from the 1 kHz repetition rate Ti:Sa laser system. The recombined beams were focussed into the absorption cell by a toroidal mirror. The transmitted XUV pulses were analyzed with a flat-field spectrometer coupled to a multichannel plate/phosphor

a)Electronic mail: jochen.mikosch@mbi-berlin.de

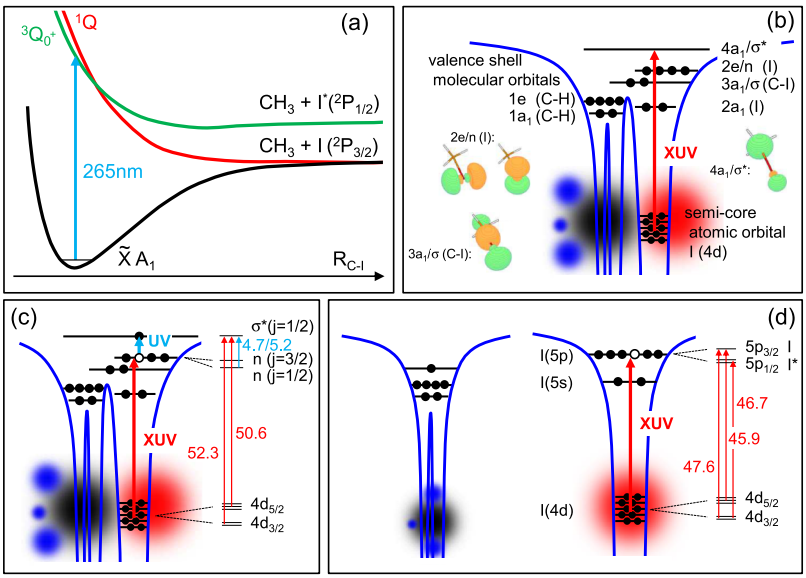

FIG. 1. (a) Schematic potential energy curves along the R_{C-I} coordinate for CH_3I A-band photodissociation. (b) XUV absorption into the σ^* LUMO orbital from the ground-state of CH_3I. The depicted SCF-HF orbitals are obtained with an aug-cc-pVDZ basis set. (c) and (d) $N_{4,5}$-edge XUV transitions in UV-pumped and dissociated CH_3I (energies in eV). HOMO-LUMO excitation by the UV laser will lead to a reduction of XUV core absorption into the σ^* LUMO (b), while creating the possibility for XUV core absorption into the HOMO (c).

screen stack and a digital camera. The spectrometer was calibrated using an aluminium filter's $L_{2,3}$-edge and known absorption lines of argon. To minimize the influence of XUV spectral fluctuations, static and pump-probe absorption spectra were recorded in quick alternation using a chopper wheel. The linear absorption difference signal was transformed to a change of absorbance (ΔA) by taking its (base-10) logarithm. A small contribution of scattered light was subtracted. The observed linewidths in CH_3I are consistent with a spectral resolution of 0.3-0.4 eV. To determine the UV-XUV cross correlation and zero time-delay, the control of autoionization line shapes of argon by semi-strong UV pulses was recorded accompanying each measurement.[11,22] In Figs. 3 and 5 the renormalized absolute peak area of the UV on/off difference of the $3s^23p^6 \rightarrow 3s3p^6np$ transition at 28 eV is plotted in grey. Taking into account the 23.3 fs lifetime,[11] cross correlations of (103 ± 6) fs and (110 ± 6) fs were extracted for the CH_3I and C_6H_5I measurements, dominated by the duration of the chirped 265 nm pulses.

Fig. 2(a) shows the XUV absorption spectrum of ground-state CH_3I, obtained as the difference of a spectrum recorded with and without CH_3I in the target cell. It is very similar to the reference spectrum from the literature,[23] obtained with (e,e) spectroscopy. The three fully resolved peaks are fitted with Voigt profiles and a static background. Their mean energies agree well with the literature values[23] (see Table I). The dominant peaks are the iodine spin-orbit doublet at 50.6 and 52.4 eV, assigned to the molecular $4d_{5/2} \rightarrow \sigma^*$ and $4d_{3/2} \rightarrow \sigma^*$ transitions (see Fig. 1(c)). Additional partially resolved features belong to transitions to higher valence orbitals (markers in Fig. 2 and Table I). In Fig. 2(b), we show the spectral change in absorbance of the dissociated CH_3I with respect to the unpumped molecule (the photodissociation action spectrum). The dominant peaks from the ground-state spectrum (A, B) are depleted (4, 5), while a strong new doublet appears at 45.9 and 46.7 eV (1, 2). These lines correspond to $4d_{5/2}(^2P_{3/2}) \rightarrow 5p_{3/2}(^2D_{5/2})$ and $4d_{3/2}(^2P_{1/2}) \rightarrow 5p_{1/2}(^2D_{3/2})$, transitions in atomic I and I* (Fig. 1(d), Table I). A very weak peak at 47.6 eV is assigned to the I: $4d_{3/2}(^2P_{3/2}) \rightarrow 5p_{3/2}(^2D_{3/2})$ transition, which is known to be nine times weaker than the I transition at 45.9 eV.[24,25] The peak areas scale linearly with pump intensity, confirming a 1-photon transition.

The excited atom fraction of the iodine photodissociation products $\Phi_{I^*} = [I^*]/([I] + [I^*])$ can be extracted from the fitted peak areas in the action spectrum, after scaling with the respective oscillator strengths (see Table I). Using the atomic spin-orbit doublet assigned to I and I* (peaks 1,2), $\Phi_{I^*}, = 0.73\pm^{0.01}_{0.03}$ is obtained. The top value (±0.01) is the

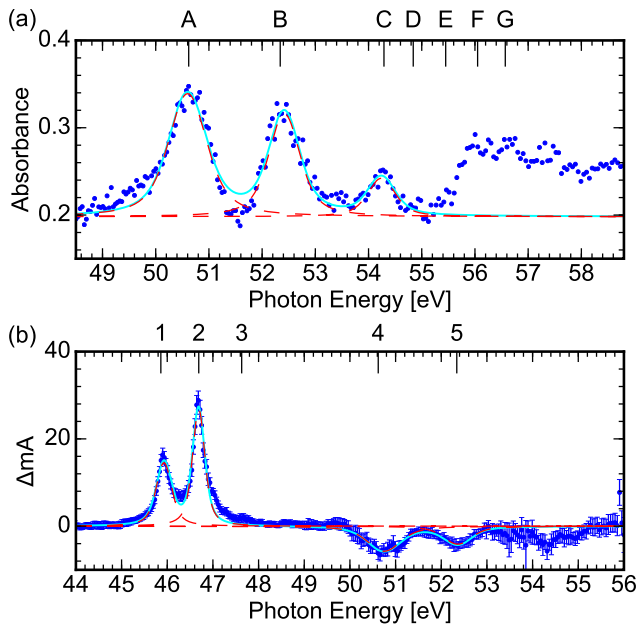

FIG. 2. (a) XUV absorption spectrum of ground-state CH_3I and (b) action spectrum of dissociated CH_3I following pumping at 265 nm (blue). The photodissociation action spectrum is averaged over differential static and pump-probe transient absorption spectra from a pump-probe delay scan, with XUV arriving 100-480 fs after the UV pump pulse. Photodissociation is complete at these delays.[26] The cyan lines are the fitted spectra using Voigt profiles (dashed red lines). The labeled vertical lines indicate the transitions assigned in Table I.

TABLE I. Fitted energetic positions (FWHM widths) of the peaks in the spectra of Fig. 2, their comparison with literature values, literature oscillator strengths f (relative errors), and the spectroscopic assignment.[23,25,27,28]

	$E_{fit}(\Gamma)$ [eV]	$E_{ref}(\Gamma)$ [eV]	f (σ_{rel})	Assignment
A	50.6(0.9)	50.62(0.9)	0.060 (5%)	CH_3I: $4d_{5/2}(I) \rightarrow \sigma^*$
B	52.4(0.7)	52.34(0.9)	0.043 (5%)	CH_3I: $4d_{3/2}(I) \rightarrow \sigma^*$
C	54.2(0.6)	54.29(0.9)	0.016 (5%)	CH_3I: $4d_{5/2}(I) \rightarrow 6p\,e$
D	...	54.84(0.9)	0.010 (5%)	CH_3I: $4d_{5/2}(I) \rightarrow 6p\,a_1$
E	...	55.45(0.9)	0.004	CH_3I: $4d_{5/2}(I) \rightarrow 7p$
F	...	56.05(0.9)	0.019	CH_3I: $4d_{3/2}(I) \rightarrow 6p\,e$
G	...	56.57(0.9)	0.014	CH_3I: $4d_{3/2}(I) \rightarrow 6p\,a_1$
1	45.9(0.4)	45.94(0.17)	0.265 (20%)	I: $4d_{5/2}(I) \rightarrow 5p_{3/2}$
2	46.7(0.3)	46.70(0.16)	0.146 (20%)	I^*: $4d_{3/2}(I) \rightarrow 5p_{1/2}$
3	...	47.64	0.029	I: $4d_{3/2}(I) \rightarrow 5p_{3/2}$
4	50.8(1.1)	50.62(0.9)	0.060 (5%)	CH_3I: $4d_{5/2}(I) \rightarrow \sigma^*$
5	52.4(0.9)	52.34(0.9)	0.043 (5%)	CH_3I: $4d_{3/2}(I) \rightarrow \sigma^*$

uncertainty due to the fit errors, while the bottom value (±0.03) arises from the uncertainty of the relative oscillator strength from the literature.[25] Alternatively, the depleted molecular transitions measure the relative CH_3I photodissociation yield, giving $\Phi_{I^*,} = 1 - \Phi_{I,} = 0.76 \pm^{0.02}_{0.05}$ (using peaks 1 and 4) and $0.74 \pm^{0.03}_{0.05}$ (peaks 1 and 5). All values are consistent within the error bars, with a mean of $\Phi_{I^*} = 0.74 \pm 0.06$, centered in the range 0.70 - 0.81 reported in the literature for 265 nm photodissociation.[20]

In Fig. 3 integrated peak areas from the action absorption spectra are shown as a function of pump-probe delay. The atomic I and I^* lines (1 and 2 in Fig. 2(b)) rise and the iodine transitions in CH_3I (sum of lines 4 and 5) are depleted immediately upon UV photon absorption within the experimental time-resolution. This important result is explained by inspecting the valence shell molecular orbitals (Fig. 1(b)). The A-band excitation drives a transition from the Highest Occupied Molecular Orbital to the Lowest Unoccupied Molecular Orbital (HOMO to LUMO). The resulting $(2e)^{-1}$ hole immediately provides a new target for XUV absorption from the iodine 4d core. Since the $(2e)^{-1}$ hole is centered on the iodine atom (see inset of Fig. 1(b)), the oscillator strength is increased as compared to the $4a_1$ target (see inset) and the positive ΔA associated with the re-filling of this hole exceeds the negative ΔA associated with the $4d \rightarrow \sigma^*$ transition (Fig. 2(b)). Since UV excitation populates $4a_1$, the depletion of the iodine transitions in CH_3I is also immediate. The valence shell of the atomic iodine product consists of a fully occupied $5s^2$ shell and a $5p^5$ shell with a single vacancy. The atomic $5s^2$ shell originates predominantly from the $2a_1$ orbital of CH_3I.[18] The $5p^5$ shell is formed from the depleted 2e(n) shell (3 electrons and 1 hole) and the $3a_1(\sigma)$ shell (2 electrons) (see Fig. 1). Importantly, since the UV-depleted 2e shell of the molecule corresponds to iodine lone pairs, which are not involved in chemical bonding, the energy shift between the 2e shell and the atomic 5p shell is expected to be small. The hole created by the pump pulse is hence expected to persist, with minor adjustment during dissociation.

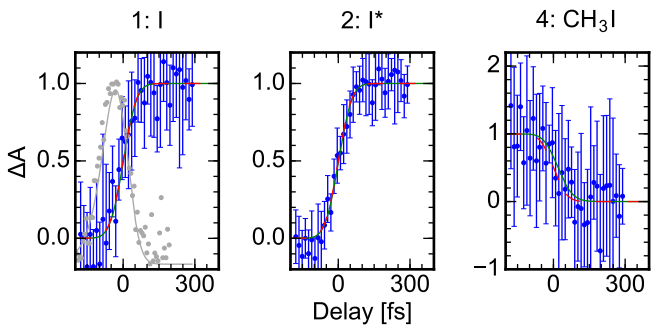

FIG. 3. Integrated peak areas (ΔA), from action spectra, as a function of pump-probe delay (blue) for CH_3I photodissociation. Integration ranges are 45.45-46.3 eV (peak 1, I), 46.3-47.25 eV (peak 2, I^*), and 50.0-53.0 eV (peaks 4,5, CH_3I). Green lines represent fits of exponential growth functions convoluted with the Gaussian Instrument Response Function (IRF, red) and are indistinguishable from the latter within our time-resolution. ΔA was renormalized to the 0-1 range. The grey curve indicates the zero time-delay and XUV-UV cross correlation (see text).

An independent particle model is convenient for rationalizing the direction of the energetic shifts of the emerging XUV transitions upon dissociation.[17] At CH_3I equilibrium bond length the $4d \rightarrow n(I)$ transition should appear at energies corresponding to the difference between the $4d(I) \rightarrow \sigma^*$ and $n(I) \rightarrow \sigma^*$ transitions. Upon dissociation, the XUV transitions converge to the atomic transitions (see Fig. 1). The 4d core is split into a $4d_{3/2}$ spin-orbit manifold and a $4d_{5/2}$ spin-orbit manifold. The I(5p) atomic state is split into $5p_{3/2}$ and $5p_{1/2}$, and the 2e(I) molecular orbitals are split into $n_{3/2}$ and $n_{1/2}$. The $^3Q_{0^+}$ A-band branch represents a $n_{1/2} \rightarrow \sigma^*$ transition, with a transition energy of 4.7 eV[20] and leads asymptotically to the I^* product, i.e., $(n_{1/2})^{-1}$ in the molecule correlates to $(5p_{1/2})^{-1}$ in the atom. Hence, at equilibrium bond length an XUV transition should appear at (52.3 -4.7) eV = 47.6 eV and converge to 46.7 eV in the asymptotic region (see Figs. 1(c) and 1(d)). In an atom, the $4d_{5/2} \rightarrow 5p_{1/2}$ transition is forbidden. The analysis given for the triplet branch $^3Q_{0^+}$ can be repeated for the singlet branch $^1Q_1$, which leads to the I ground state product. Since the C–I coordinate-dependent potential energy surfaces of the core-excited states are not known, we take the energetics at the equilibrium bond length for this estimate. $^1Q_1$ corresponds to $n_{3/2} \rightarrow \sigma^*$, with a transition energy of 5.2 eV and correlates to $(5p_{3/2})^{-1}$ in the atom. Hence, at the equilibrium bond length XUV transitions should appear at (50.6-5.2) eV = 45.4 eV and (52.3-5.2) eV = 47.1 eV and converge to 45.9 eV and 47.6 eV, respectively, in the asymptotic region. Note that the 45.9 eV transition is nine times more intensive (Table I). In summary, the independent particle model predicts that the dominant asymptotic XUV lines I: $4d\,(^2P_{3/2}) \rightarrow 5p\,(^2D_{5/2})$ and I^*: $4d\,(^2P_{1/2}) \rightarrow 5p\,(^2D_{3/2})$ at 45.9 eV and 46.7 eV reach their final position via a sub-eV shift to higher (45.4 to 45.9 eV) and lower energies (47.6 to 46.7 eV), respectively.

For each time step in the pump-probe delay scan, we fit Voigt profiles to the dominant emerging XUV transitions and plot the center positions as a function of time-delay (Fig. 4). In line with the expectation from the independent particle model, we find a clear, small shift to lower energies for the dominant I^* transition and to somewhat higher energies for the dominant I transition. The shifts are about −0.15 eV (I^*) and +0.10 eV (I), i.e. less than expected, but showing the predicted relative

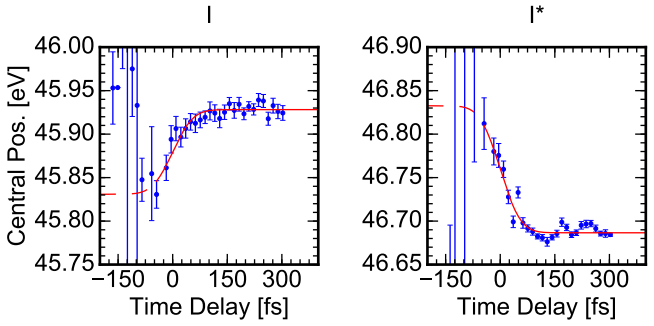

FIG. 4. Pump-probe delay time dependence (blue) of the energy mean of the dominant emerging I and I* XUV transitions (lines 1 and 2) for CH_3I photodissociation. The Gaussian IRF is depicted in red, fits of convoluted exponential growth functions are indistinguishable from it within our time-resolution.

trend. Smaller measured than expected shifts may be partly due to the long UV pulse duration on the time scale of the dynamics. In fact, a fit of a convolution of an exponential growth/decay function and the fixed Gaussian IRF shows no significant time-constant of the shifts of the XUV lines within our experimental resolution, as is the case for the emergence of these transitions (see above).

The very rapid emergence and shift of the new XUV transitions is in marked contrast to the ≈90 fs rise time of the atomic mass signal in femtosecond UV pump - multi-photon ionization probe experiments.[26] While the latter probe the asymptotic atomic products, the shifts of the emerging XUV transitions represent the relaxation of the valence shell vacancy, which we find to take place during the very first moments of dissociation.

We now turn to iodobenzene, which features a delocalized π-system, responsible for a large fraction of the UV oscillator strength. Low-lying excitations of C_6H_5I include dissociative $\pi \rightarrow \sigma^*$ and bound $\pi \rightarrow \pi^*$ transitions, as well as the $n \rightarrow \sigma^*$ transitions also found in iodomethane. The mixed A-band is located in the 240-320 nm range[29] and leads to production of I* ($\tau \approx 350$ fs), I ($\tau \approx 350$ fs, dominant channel) and I ($\tau \approx 700$ fs, weak channel) fragments.[30–33] The main doorway state at 265 nm is $^3B_1$ ($\pi \rightarrow \sigma^*$ transition).[34] The $^3B_1$ potential energy surface is repulsive along the C–I coordinate, asymptotically forming ground state I. It crosses with the repulsive $^5B_1$ and $^5A_2$ states, which also converge to I, and with the repulsive $^4A_1$ state, which produces I*. The slow channel is believed to originate from the initial excitation of the predissociative $^4B_2$ ($\pi \rightarrow \pi^*$) state, which undergoes an intersystem crossing.[34] At 265 nm, the $1A_1 \rightarrow 4B_2$ oscillator strength is an order of magnitude below that of $1A_1 \rightarrow 3B_1$, consistent with the direct dissociation accounting for 84% of the total yield.[33]

In Fig. 5(a) we show the XUV action spectrum of iodobenzene photodissociation at 265 nm (cf. Fig. 2(b)). A depleted molecular transition at 50.6 eV $(4d_{5/2})^{-1}$ is observed. We hence expect the $(4d_{3/2})^{-1}$ counterpart at 52.3 eV, where indeed evidence of a peak is visible. The atomic I: $4d_{5/2} \rightarrow 5p_{3/2}$ transition at 45.9 eV is much stronger than the I*: $4d_{3/2} \rightarrow 5p_{1/2}$ transition at 46.7 eV. Furthermore the I: $4d_{3/2} \rightarrow 5p_{3/2}$ transition at 47.6 eV is now clearly visible

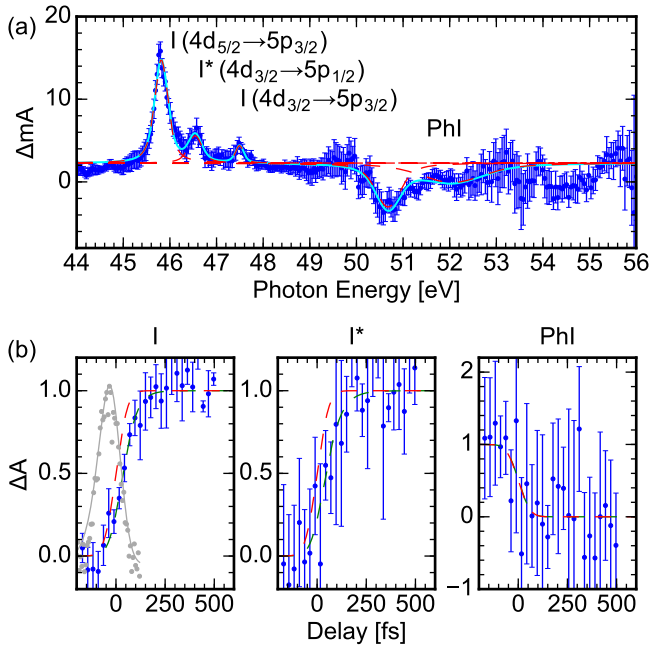

FIG. 5. (a) XUV action spectrum for iodobenzene photodissociation at 265 nm. The spectrum is averaged over transient pump-probe spectra, with XUV arriving 195-515 fs after the UV pulse. Blue is experimental data, cyan a fit using five Voigt profiles (red). (b) Integrated intensity of the dominant peaks as a function of pump-probe delay time. Green lines represent fits of exponential growth functions convoluted with the Gaussian IRF, shown in red. The grey curve indicates the zero time-delay and XUV-UV cross correlation (see text).

and has the expected relative intensity. Fitting peak areas and scaling with the relative oscillator strength (Table I), we obtain $\Phi_{I^*} = 0.33\pm^{0.03}_{0.03}$, in good agreement with the previously reported experimental value of $\Phi_{I^*} = 0.32 \pm 0.05$ from Sage *et al.*[16]

Fig. 5(b) shows the evolution of the integrated peak areas as a function of pump-probe delay. The iodine transitions in the bound molecule are depleted on a time scale indistinguishable from the cross correlation (panel PhI), as was the case in CH_3I. Interestingly, the atomic features appear with noticeable delay, namely, with rise times of (40 ± 9) fs and (53 ± 31) fs for I and I*, respectively. The position of the emerging I peak at 45.9 eV is independent of time-delay in contrast to the CH_3I case; for the weaker transition in I* the signal-to-noise level and proximity of the intense I peak precludes an analysis of the shift.

While a detailed explanation has to be deferred to a later publication and involve theory, we can speculate on the marked difference observed between the two molecules. In contrast to CH_3I, the dominant $\pi \rightarrow \sigma^*$ UV excitation in iodobenzene creates a vacancy, which is not localized on the reporter atom but rather the distant phenyl ring. Therefore, it is initially not accessible for a vertical XUV transition from the iodine core. An evolution of the valence shell is necessary for the hole to migrate and the new XUV transitions, which converge to the asymptotic atomic lines, to emerge. On the other hand, the unoccupied orbital in the ground-state C_6H_5I is populated immediately with UV absorption, indicating dominant σ^* character of the UV-excited state. The absence of a time-dependent shift for the transition

converging to I: $4d_{5/2} \rightarrow 5p_{3/2}$ may also be understood within the independent particle model as follows: The transition energy for the dominant UV excitation $1A_1 \rightarrow 3B_1$ is 4.5 eV.[34] Therefore at the equilibrium bond length the XUV transition should appear at (50.6-4.5) eV = 46.1 eV and converge to 45.9 eV in the asymptotic region. Given the time-delay of the transition and smaller than expected shifts for CH_3I, the shift is probably too small to be observed in our current experiment. Consistent with the case of CH_3I the emergence of the XUV transitions is still much faster than the rise time of the atomic mass signal in femtosecond photoionization experiments (350 fs for the dominant direct channel[32]).

In their recent comparable work on CH_3I, Attar *et al.* find weak shoulders upon the emerging atomic iodine transitions, which subsequently disappear during the dissociation.[17] After subtracting the scaled atomic transitions, the shoulders are interpreted as new, short-lived intermediate core-to-valence electronic states at distinct XUV energies which are assigned to the transition-state region. These transient resonances are found to reach a maximum at ≈40 fs and decay within ≈90 fs. Our experimental raw data for CH_3I appear to be consistent with the data of Attar *et al.* While we cannot rule out such distinct transient intermediate resonances in CH_3I, we believe that our interpretation of the data as a weak energy shift of the valence shell hole is a straightforward alternative that should be considered. The much shorter time scales as compared to complete dissociation[26] suggest that in CH_3I very little nuclear motion is involved in the relaxation of the valence shell vacancy, attributed to its nature originating from the iodine lone pair. In view of the marked difference observed for iodobenzene, XUV transient absorption is anticipated to be sensitive to the coupled electronic and structural dynamics in molecules. In contrast to time-resolved photoelectron spectroscopy,[35] the dynamics is projected on sparse core-excited states rather than dense cation states, which offers a different coordinate dependence. The recent development of theoretical methods dedicated to femtosecond NEXAFS of molecular dynamics[36] is hence very timely; it will aid to reach a detailed understanding of the results obtained in the current groundbreaking experiments.

We thank Oleg Kornilov (MBI) for help with the laser system, fruitful discussions, and comments on the manuscript. We also thank Gerry O'Sullivan (UCD, Ireland) for helpful discussion on XUV absorption cross sections of iodine, Rune Lausten (NRC, Canada) for technological advise and Roman Peslin (MBI) for excellent technical assistance. G.R. thanks the Netherlands Organization for Scientific Research (NWO) for financial support (Rubicon 68-50-1410).

[1]F. Krausz and M. Ivanov, Rev. Mod. Phys. **81**, 163 (2009).
[2]C. Bressler and M. Chergui, Chem. Rev. **104**, 1781 (2004).
[3] Stöhr, *NEXAFS Spectroscopy* (Springer, 1992).
[4]K. Hong, H. Cho, R. Schoenlein, T. Kim, and N. Huse, Acc. Chem. Res. **48**, 2957 (2015).
[5]M. Chergui, Acc. Chem. Res. **48**, 801 (2015).
[6]A. Attar, L. Piticco, and S. Leone, J. Chem. Phys. **141**, 164308 (2014).
[7]C. Milne, T. Penfold, and M. Chergui, Coord. Chem. Rev. **277**, 44 (2014).
[8]M. Vaida and S. Leone, Chem. Phys. **442**, 41 (2014).
[9]A. Bhattacherjee, A. Attar, and S. Leone, J. Chem. Phys. **144**, 124311 (2016).
[10]E. Goulielmakis, Z.-H. Loh, A. Wirth, R. Santra, N. Rohringer, V. Yakovlev, S. Zherebtsov, T. Pfeifer, A. Azzeer, M. Kling, S. Leone, and F. Krausz, Nature **466**, 739 (2010).
[11]H. Wang, M. Chini, S. Chen, C.-H. Zhang, F. He, Y. Cheng, Y. Wu, U. Thumm, and Z. Chang, Phys. Rev. Lett. **105**, 143002 (2010).
[12]M. Holler, F. Schapper, L. Gallmann, and U. Keller, Phys. Rev. Lett. **106**, 123601 (2011).
[13]C. Ott, A. Kaldun, P. Raith, K. Meyer, M. Laux, J. Evers, C. Keitel, C. Greene, and T. Pfeifer, Science **340**, 716 (2013).
[14]A. Beck, D. Neumark, and S. Leone, Chem. Phys. Lett. **624**, 119 (2015).
[15]A. T. J. B. Eppink and D. H. Parker, J. Chem. Phys. **110**, 832 (1999).
[16]A. Sage, T. Oliver, D. Murdock, M. Crow, G. Ritchie, J. Harvey, and M. Ashfold, Phys. Chem. Chem. Phys. **13**, 8075 (2011).
[17]A. Attar, A. Bhattacherjee, and S. Leone, J. Phys. Chem. Lett. **6**, 5072 (2015).
[18]R. Mulliken, J. Chem. Phys. **8**, 382 (1940).
[19]A. Gedanken and M. D. Rowe, Chem. Phys. Lett. **34**, 39 (1975).
[20]A. Alekseyev, H.-P. Liebermann, R. Buenker, and S. Yurchenko, J. Chem. Phys. **126**, 234102 (2007).
[21]C. Neidel, J. Klei, C.-H. Yang, A. Rouzee, M. Vrakking, K. Klunder, M. Miranda, C. Arnold, T. Fordell, A. L'Huillier, M. Gisselbrecht, P. Johnsson, M. Dinh, E. Suraud, P.-G. Reinhard, V. Despre, M. Marques, and F. Lepine, Phys. Rev. Lett. **111**, 033001 (2013).
[22]B. Bernhardt, A. Beck, X. Li, E. Warrick, M. Bell, D. Haxton, C. McCurdy, D. Neumark, and S. Leone, Phys.Rev.A **89**, 023408 (2014).
[23]T. Olney, G. Cooper, and C. Brion, Chem. Phys. **232**, 211 (1998).
[24]L. Nahon, A. Svensson, and P. Morin, Phys. Rev. A **43**, 2328 (1991).
[25]G. O'Sullivan, C. McGuinness, J. Costello, E. Kennedy, and B. Weinmann, Phys. Rev. A **53**, 3211 (1996).
[26]M. Corrales, V. Loriot, G. Balerdi, J. Gonzalez-Vazquez, R. de Nalda, L. Banares, and A. Zewail, Phys. Chem. Chem. Phys. **16**, 8812 (2014).
[27]G. O'Sullivan, private communication.
[28]L. Nahon, P. Morin, and F. Combet-Farnoux, Phys. Scr. **T41**, 104 (1992).
[29]S. Obrien, C. Kittrell, J. Kinsey, and B. Johnson, J. Chem. Phys. **96**, 67 (1992).
[30]H. J. Hwang and M. A. Elsayed, J. Chem. Phys. **96**, 856 (1992).
[31]D. P. Zhong and A. H. Zewail, J. Phys. Chem. A **102**, 4031 (1998).
[32]M. Kadi, J. Davidsson, A. Tarnovsky, M. Rasmusson, and E. Akesson, Chem. Phys. Lett. **350**, 93 (2001).
[33]X. Zhang, Z. Wei, Y. Tang, T. Chao, B. Zhang, and K. Lin, ChemPhysChem **9**, 1130 (2008).
[34]S.-F. Chen, F.-Y. Liu, and Y.-J. Liu, J. Chem. Phys. **131**, 124304 (2009).
[35]A. Stolow and J. Underwood, Adv. Chem. Phys. **139**, 497 (2008).
[36]S. Neville, V. Averbukh, S. Patchkovskii, M. Ruberti, R. Yun, M. Chergui, A. Stolow, and M. Schuurman, "Beyond Structure: Ultrafast X-Ray Absorption Spectroscopy as a Probe of Non-Adiabatic Wavepacket Dynamics" (submitted).